

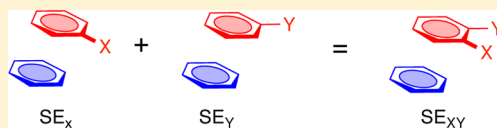
Additivity of Substituent Effects in Aromatic Stacking Interactions

Jungwun Hwang, Ping Li, William R. Carroll,[†] Mark D. Smith, Perry J. Pellechia, and Ken D. Shimizu*

Department of Chemistry and Biochemistry, University of South Carolina, Columbia, South Carolina 29208, United States

S Supporting Information

ABSTRACT: The goal of this study was to experimentally test the additivity of the electrostatic substituent effects (SEs) for the aromatic stacking interaction. The additivity of the SEs was assessed using a small molecule model system that could adopt an offset face-to-face aromatic stacking geometry. The intramolecular interactions of these molecular torsional balances were quantitatively measured via the changes in a *folded/unfolded* conformational equilibrium. Five different types of substituents were examined (CH₃, OCH₃, Cl, CN, and NO₂) that ranged from electron-donating to electron-withdrawing. The strength of the intramolecular stacking interactions was measured for 21 substituted aromatic stacking balances and 21 control balances in chloroform solution. The observed stability trends were consistent with additive SEs. Specifically, additive SE models could predict SEs with an accuracy from ± 0.01 to ± 0.02 kcal/mol. The additive SEs were consistent with Wheeler and Houk's direct SE model. However, the indirect or polarization SE model cannot be ruled out as it shows similar levels of additivity for two to three substituent systems, which were the number of substituents in our model system. SE additivity also has practical utility as the SEs can be accurately predicted. This should aid in the rational design and optimization of systems that utilize aromatic stacking interactions.



INTRODUCTION

Aromatic stacking interactions play an important role in determining the structure, property, and function of many synthetic^{1–4} and biological systems.^{4–7} For example, attractive interactions of aromatic surfaces have been cited as a major stabilizing interaction in nucleic acid and protein structures,⁸ host–guest complexes,^{9,10} solid-state structures,¹¹ and transition states of asymmetric catalysts.^{12,13} A common strategy for modulating the strengths of aromatic stacking interactions is via the introduction of substituents on the aromatic rings. Theoretical^{14–18} and experimental^{19–22} studies have found that electron-withdrawing groups stabilize and electron-donating groups generally destabilize aromatic stacking interactions. In addition, theoretical studies have predicted that the electronic substituent effects (SEs) in multisubstituted aromatic rings will be additive.²³ For example, Sherrill et al. demonstrated an excellent linear correlation between the interaction energy and the number of substituents. However, these theoretical studies were carried out *in vacuo* and examined the aligned face-to-face stacking geometry, where one aromatic ring is directly over the opposing ring. In this study, we experimentally test whether the electrostatic SEs are additive for the more commonly observed offset aromatic stacking geometry (Figure 1). SE additivity would provide a simple means of rationally designing systems that utilize aromatic

stacking and aid in rational design of host–guest, drug–receptor, and substrate–catalysts systems that incorporate aromatic stacking interactions. In addition, the verification of additive SEs could help differentiate the different theoretical models of the aromatic stacking SEs.^{24–28}

Our strategy was to prepare and study a series of small molecule model systems (Scheme 1), which could form and

Scheme 1. Representation of (a) the Molecular Torsional Balance Designed To Measure the SEs of an Intramolecular Aromatic Stacking Interaction via Changes in the *Folded/Unfolded* Equilibrium Ratio and (b) the Control Balance Designed to Measure the Solvent and Repulsive Lone Pair to π Interactions of the Oxygen Linker

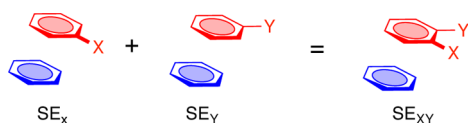
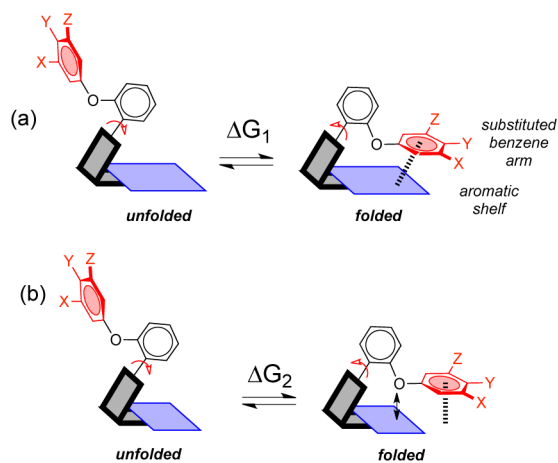


Figure 1. General depiction of additive SEs for aromatic stacking interaction in the offset face-to-face geometry.

Received: May 1, 2014

measure the strength of an intramolecular offset face-to-face (or parallel) aromatic stacking interaction. Five different substituents (OCH₃, CH₃, Cl, CN, NO₂) were introduced on the aromatic ring yielding a total of 21 different combinations. This range of substituents and substitution patterns allowed us to systematically test whether the SEs of the monosubstituted systems could be added together to accurately predict the SEs for the multisubstituted systems (Figure 1).

There have been a number of experimental studies that have examined the additivity of SEs in face-to-face aromatic stacking interactions. However, these previous studies examined a limited number of substituents, measured the interaction energies via an indirect method, and yielded to opposing conclusions. Two separate studies examined the additivity of SEs in aromatic stacking interactions indirectly via measuring changes in a rotational barrier. Cozzi and Siegel showed that benzene rings with varying numbers of fluorines appeared to show SE additivity for the stacking interaction within a rigid 1,8-diarylnaphthalene model system.²⁹ Conversely, Waters and Rashkin found that the SEs for CH₃, CF₃, and F groups fell short of additivity by an average of 19% in their benzylpyridinium model system.²² A possible explanation for the opposing conclusions is the indirect method of measuring aromatic stacking energies used in both studies. The face-to-face aromatic stacking interaction energies in the ground states were measured via the rotational barrier of one of the aromatic surfaces. However, both systems could form additional edge-to-face or edge-to-substituent interactions in their transition states. Therefore, the observed SE trends could be a combination of the trends for the face-to-face and these other interactions. Another experimental study of note is Schneider's comprehensive study of the SEs in the host-guest interactions of porphyrins in water.³⁰ The observed additive SEs were attributed to dispersion and solvophobic effects as opposed to aromatic stacking interactions.

Our recently reported molecular torsional balance model system (Scheme 1 and Figure 2) has a number of attractive

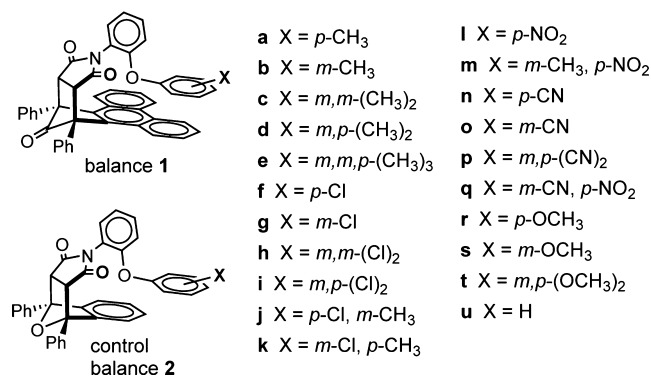


Figure 2. *Folded* conformers of aromatic stacking balance 1 and nonstacking control balance 2, which contain 21 different substituted benzenes arms (a–u).

attributes for the study of SE additivity.^{31,32} First, we previously established that this rigid bicyclic model system forms a well-defined intramolecular aromatic stacking interaction in the *folded* conformer. The X-ray crystal structure (Figure 3) showed that the aromatic surfaces of the phenyl ether arm and the phenanthrene shelf were held in a parallel geometry and at a proper distance (3.76 Å, centroid-to-plane). Second, the aromatic stacking energy can be easily and accurately

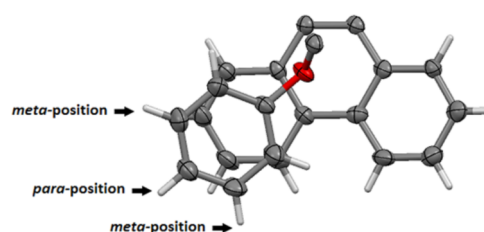


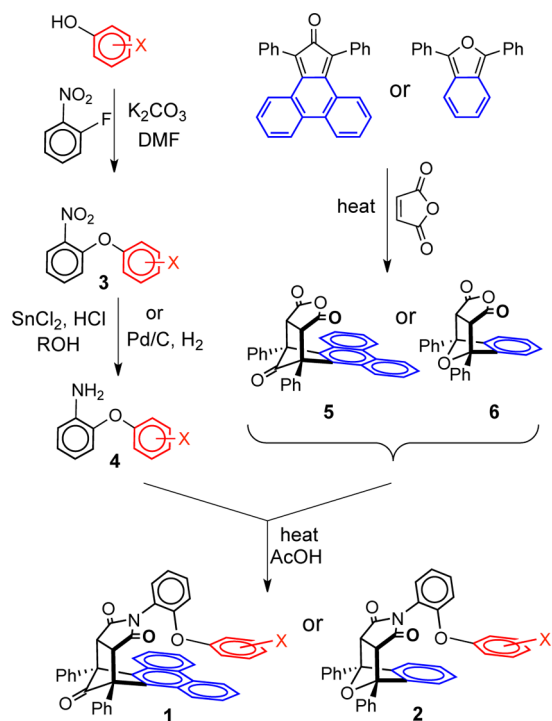
Figure 3. Top view of the *folded* conformer of the X-ray crystal structure of a two-armed version of unsubstituted balance 1 highlighting the intramolecular aromatic stacking interaction between the phenyl ether of the arm (top) and the phenanthrene shelf (bottom).³¹ For clarity, the bicyclic framework is hidden.

measured via a conformational equilibrium (Scheme 1). Due to restricted rotation around the C_{aryl}–N_{imide} single bond, 1 and 2 adopt distinct *folded* and *unfolded* conformers that form and break the intramolecular stacking interaction. Thus, the *folded*/*unfolded* conformer ratio provides a sensitive (± 0.008 to ± 0.03 kcal/mol) measure of the interaction.^{33,34} This ratio was easily measured from the peak areas of the two conformers in the ¹H NMR spectra, which were in slow exchange at room temperature. Third, the balance exclusively forms the face-to-face geometry and cannot form alternative stacking geometries due to the rigidity of the bicyclic framework. Molecular modeling simulations confirmed that there was insufficient distance between the aromatic surfaces in the *folded* conformer to form the edge-to-face geometry. Fourth, we could introduce up to three substituents on the arm of the balance that would only electrostatically attenuate the stacking interaction. The X-ray structure (Figure 3) showed that substituents at these positions could not form steric or dispersion interactions with the aromatic shelf. Due to the offset geometry, the benzene arm juts out beyond the edge of the phenanthrene shelf, and substituents at the *para*- and *meta*-positions are not over the aromatic shelf. The elimination of these secondary interactions was important, as experimental^{24,22} and theoretical studies³⁵ have shown that they can disrupt the electrostatic SE trends of interest. While the crystal structure shows the two *meta*-positions are in different geometries, they are equivalent on the NMR time scale. This is because, as shown by calculations by Datta et al.,³⁶ the arm is moving back and forth rapidly between the two outer benzenes of the phenanthrene shelf.

Finally, control balances 2a–u could be used to measure and remove other possible influences on the *folded*/*unfolded* ratios in balance 1. These included repulsive the lone pair to π interactions of the oxygen linker^{31,36,37} or solvent effects of the substituted aryl ether arms.^{38,39} The control balances 2a–u contained the same substituted aromatic arms but had a smaller benzene shelf that could not form the aromatic stacking interactions. This can be visualized using the crystal structure in Figure 3. The control balance 2 contains only the central benzene ring of the phenanthrene shelf in 1, which can form lone pair to π interactions with the linker ether oxygen. Thus, the aromatic interaction energies were measured using the difference in the folding energies of the aromatic stacking balances 1 and the control balances 2 ($\Delta G_1 - \Delta G_2$).

RESULTS AND DISCUSSION

First, the 21 substituted balances 1a–u and the matching 21 substituted control balances 2a–u (Figure 2) were prepared. These were all rapidly and efficiently assembled using a common modular synthesis route (Scheme 2). The substituted

Scheme 2. Modular Synthetic Route Used to Prepare Balances 1 and 2 with Substituted Arms a–k, n, o, r–t

aromatic ring of the arms and the aromatic shelves were synthesized independently and then condensed together in the last step. Five representative substituents were chosen spanning the range from electron-donating (CH_3 , OCH_3) to electron-withdrawing (Cl , CN , and NO_2).⁴⁰ A variety of substitution patterns were examined including 1 unsubstituted (**1u**), 9 monosubstituted (**1a**, **b**, **f**, **g**, **n**, **o**, **r**, **s**), 10 disubstituted (**1c**, **d**, **h–m**, **p**, **q**, **t**), and 1 trisubstituted (**1e**) arms.

All of the aromatic arms **4** were assembled via an $\text{S}_{\text{N}}\text{Ar}$ reaction. The majority of the arms (**4a–k**, **n**, **o**, **r–t**) were made by the reaction of the appropriately substituted phenolate with 2-fluoronitrobenzene to form diphenyl ethers **3**. Then 2-nitro groups were reduced to the primary amines. For arms with strong electron-withdrawing substituents (**l**, **m**, **p**, **q**), their phenolates were not sufficiently nucleophilic. Therefore, **4l**, **m**, **p**, **q** were prepared in one step via the $\text{S}_{\text{N}}\text{Ar}$ reaction of 2-aminophenol with the appropriately substituted fluoro- or nitrobenzene (not shown).

The aromatic shelves were synthesized via the Diels–Alder reaction of maleic anhydride with either phenylcyclohexene or diphenylisobenzofuran to yield the *endo*-bicyclic anhydrides **5** or **6** containing phenanthrene or benzene surfaces.⁴¹ Finally, thermal condensation reaction of a substituted aniline arm (**4a–u**) and a bicyclic anhydride shelf (**5** or **6**) yielded the *endo*-bicyclic **1** and **2**.

The ability of balances **1** and **2** to form the desired intramolecular aromatic stacking interactions was established by ^1H NMR. The expected upfield shifts were observed for the protons on the substituted benzene arms of **1a–u**, which were indicative of the benzene arm being positioned over the phenanthrene shelf. In particular, the *ortho*-protons (adjacent to the ether oxygen) of the benzene arms shifted from 1.0 to 1.2 ppm upfield. By comparison, upfield shifts were not observed for the benzene arm protons of control balances **2a–u**, which

have a shorter benzene shelf that cannot form intramolecular aromatic stacking.

The ability to measure the intramolecular stacking interactions was confirmed by examination of the ^1H NMR spectra. The presence of distinct *folded* and *unfolded* conformers was observed via the separate set of peaks in the ^1H NMR spectra (CDCl_3 , 25°C) for most of the protons in **1a–u** and **2a–u**. Thus, the two conformers were in slow exchange, and *folded/unfolded* ratio could be easily measured from the corresponding peak areas. The succinimide methine protons were used for this analysis because they were singlets in a relatively clear region of the spectra (4.2–4.7 ppm). To ensure the accuracy and consistency of the measurement, the line-fitting method was applied to high-concentration NMR samples (30 mM).^{42,43} In this manner, the *folded/unfolded* ratios for **1** and **2** were measured (Table 1), and the corresponding folding energies (ΔG_1 and ΔG_2) were calculated.

Table 1. Measured Folding Energies (kcal/mol) of Balances 1 (ΔG_1) and Control Balances 2 (ΔG_2) Systems and SEs ($\text{SE}_x = (\Delta G_{1x} - \Delta G_{2x}) - (\Delta G_{1u} - \Delta G_{2u})$)

arm	substituents	ΔG_1^a	ΔG_2^a	$\text{SE}_{\text{meas}}^b$
a	<i>m</i> - CH_3	0.40	1.50	−0.19
b	<i>p</i> - CH_3	0.44	1.31	0.05
c	<i>m,m</i> - $(\text{CH}_3)_2$	0.29	1.56	−0.35
d	<i>m,p</i> - $(\text{CH}_3)_2$	0.35	1.35	−0.08
e	<i>m,m,p</i> - $(\text{CH}_3)_3$	0.34	1.52	−0.27
f	<i>p</i> -Cl	0.15	1.22	−0.15
g	<i>m</i> -Cl	−0.02	1.45	−0.54
h	<i>m,m</i> - $(\text{Cl})_2$	−0.46	1.38	−0.92
i	<i>m,p</i> - $(\text{Cl})_2$	−0.37	1.28	−0.73
j	<i>p</i> -Cl, <i>m</i> - CH_3	0.03	1.25	−0.30
k	<i>m</i> -Cl, <i>p</i> - CH_3	−0.01	1.30	−0.39
l	<i>p</i> - NO_2	0.22	1.51	−0.36
m	<i>p</i> - NO_2 , <i>m</i> - CH_3	−0.28	1.58	−0.94
n	<i>p</i> -CN	0.24	1.47	−0.31
o	<i>m</i> -CN	−0.24	1.31	−0.63
p	<i>m,p</i> - $(\text{CN})_2$	−0.31	1.61	−1.00
q	<i>p</i> - NO_2 , <i>m</i> -CN	0.34	1.26	0.01
r	<i>p</i> - OCH_3	0.33	1.41	−0.16
s	<i>m</i> - OCH_3	0.21	1.29	−0.15
t	<i>m,p</i> - OCH_3	0.03	1.56	−0.61
u	none	0.48	1.40	0.00

^a ΔG_1 and ΔG_2 were measured at 25°C with an error of ± 0.008 and ± 0.03 kcal/mol, respectively. ^bSE with an error of ± 0.03 kcal/mol.

The folding energies of **1** and **2** (ΔG_1 and ΔG_2) were analyzed to verify that *folded/unfolded* equilibrium provided a measure of the intramolecular aromatic stacking energies in **1**. The ΔG_1 values (−0.46 to 0.48 kcal/mol) were consistently lower in energy than the ΔG_2 values (1.22 to 1.61 kcal/mol). This was consistent with the expected stabilization of the *folded* conformer in **1** by aromatic stacking interactions. The average difference of −1.3 kcal/mol was consistent with previous measures of benzene–benzene stacking interactions in organic solution.^{20,24}

Hammett plot analyses were conducted to establish that the electrostatic SEs in our aromatic stacking model system were similar to those in previous theoretical and experimental studies.^{19–22} To isolate the intramolecular stacking energies, the difference in folding energies of **1** and **2** ($\Delta G_1 - \Delta G_2$) of the monosubstituted balances were plotted against their σ_{meta}

parameters (Figure 4). The Hammett σ_{meta} parameter was used because it more closely correlates to the purely electrostatic SEs

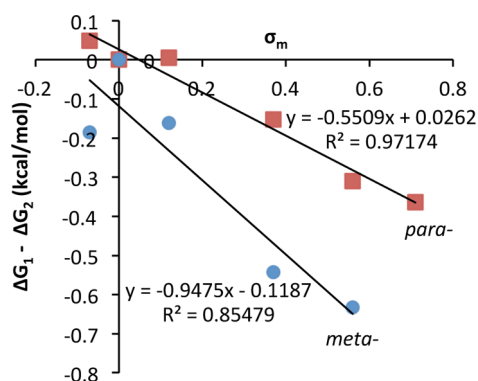


Figure 4. Hammett σ_m plot of $\Delta G_1 - \Delta G_2$ for the monosubstituted balances with substituents in the *meta*- (blue) or *para*-substituents (red) (the substituents from left to right CH_3 , H, OCH_3 , Cl, CN, NO_2).

than σ_{para} which also includes resonance effects.^{15,24} Interestingly, the *meta*- and *para*-systems displayed distinct linear trends with slopes of (-0.95 and -0.55 kcal/mol). The origins of this positional dependence will be discussed in more detail below. However, the overall sign and magnitudes of these slopes were consistent with those measured by Hunter (-0.62 kcal/mol)²¹ and Gung (-1.06 kcal/mol)²⁰ for face-to-face aromatic stacking interactions in organic solvents.

The importance of the control balances **2** in improving the accuracy of the analysis was tested by comparing the Hammett plots with ($\Delta G_1 - \Delta G_2$) and without (ΔG_1) the balance **2** corrections. Although the Hammett plots without balance **2** had similar magnitude negative slopes, there was considerably more scatter in the linear correlation. For example, the R^2 value for the *para*-substituted values for ΔG_1 was 0.69 as compared to 0.97 for $\Delta G_1 - \Delta G_2$. The improved correlation with ΔG_2 suggests that secondary factors other than the electron-withdrawing and -donating effects of the substituents influence the folding ratios in **1**. These secondary factors include solvation effects, changes in the dipoles of the *folded* and *unfolded* conformers, and resonance effects on the oxygen linker that could modulate the repulsive lone pair to π interactions.

Once the viability of our model system was established, the additivity of the SEs was assessed. The SEs in **1** were calculated using eq 1. The SE for an arm with substituents x was defined as the difference in the folding energies of **1** and **2** containing the substituents x . In addition, the $\text{SE}_{(x)}$ was normalized by subtracting out the stacking interactions in the unsubstituted balances **1u** and **2u**. Thus, the SE for the unsubstituted arm (SE_{1u}) was 0.0 kcal/mol.

$$\text{SE}_{(x)} = (\Delta G_{1x} - \Delta G_{2x}) - (\Delta G_{1u} - \Delta G_{2u}) \quad (1)$$

An initial analysis of the SE_{measd} values for the 11 multisubstituted arms in Table 2 were consistent with SE additivity. There was a good correlation between the SE_{measd} and SE_{calcd} values calculated from the sum of the SE_{measd} for the individual substituents. For example, the SE_{measd} (-0.35 kcal/mol) for the *m,m*- $(\text{CH}_3)_2$ arm **c** is very similar to the SE_{calcd} value (-0.37 kcal/mol) calculated from the sum of two SE_{measd} from the *m*- CH_3 arms. The agreement between the measured and calculated SEs spanned a diverse set of substituent types. These included arms with electron-donating CH_3 and OCH_3 ,

Table 2. Comparison of the Calculated (SE_{calcd}) and Measured (SE_{measd}) multisubstituent effects. SE_{calcd} were calculated from the sum of the SE_{measd} for the constituent mono-SE

multisubst arm	sum of monosubst $\text{SE}_{\text{measd}}^a$	$\text{SE}_{\text{calcd}}^b$	$\text{SE}_{\text{measd}}^a$
c 	$2 \times \left(\text{Structure of m-CH}_3 \right)$ (-0.19)	= -0.37	-0.35
d 	$\text{Structure of m-CH}_3 + \text{Structure of p-CH}_3$ (-0.19) (0.05)	= -0.14	-0.08
e 	$2 \times \left(\text{Structure of m-CH}_3 \right) + \text{Structure of p-CH}_3$ (-0.19) (0.05)	= -0.32 ^c	-0.27
h 	$2 \times \left(\text{Structure of m-Cl} \right)$ (-0.54)	= -1.09	-0.92
i 	$\text{Structure of m-Cl} + \text{Structure of p-Cl}$ (-0.54) (-0.15)	= -0.70	-0.73
j 	$\text{Structure of m-CH}_3 + \text{Structure of m-Cl}$ (-0.19) (-0.15)	= -0.34	-0.30
k 	$\text{Structure of m-Cl} + \text{Structure of p-CH}_3$ (-0.54) (0.05)	= -0.49	-0.39
m 	$\text{Structure of m-CH}_3 + \text{Structure of m-NO}_2$ (-0.19) (-0.36)	= -0.55	-0.61
p 	$\text{Structure of m-CN} + \text{Structure of p-CN}$ (-0.63) (-0.31)	= -0.94	-1.00
q 	$\text{Structure of m-CN} + \text{Structure of p-NO}_2$ (-0.63) (-0.36)	= -1.00	-0.94
s 	$\text{Structure of m-OMe} + \text{Structure of p-OMe}$ (-0.16) (0.01)	= -0.16	-0.15

^a SE_{measd} (kcal/mol) in CDCl_3 at 25 °C with an error of $\leq \pm 0.03$ kcal/mol. ^b SE_{calcd} of disubstituents with an error of $\leq \pm 0.04$ kcal/mol. ^c SE_{calcd} of trisubstituents with an error of $\leq \pm 0.05$ kcal/mol.

groups (arms **c**, **d**, **e**, **s**), electron-withdrawing Cl, NO_2 , and CN groups (arms **h**, **i**, **p**, **q**), and mixtures of electron-donating and withdrawing groups (arms **j**, **k**, **m**).

However, there was not perfect agreement between the measured and calculated SE values in Table 2. Therefore, additional analyses were conducted to determine whether these deviations were systematic or random error. First, a correlation plot of the calculated and measured SE values (Figure 5) showed an excellent linear correlation with an R^2 value of 0.96 and a slope near unity (0.99). The residuals ($\text{SE}_{\text{calcd}} - \text{SE}_{\text{measd}}$) had a standard error ± 0.02 kcal/mol, which was less than the error of the analysis of ± 0.03 kcal/mol. Most importantly, the SE_{measd} values were not consistently lower than the SE_{calcd} values. In addition, a plot of the residuals did not show any systematic variations. Specifically, the residuals for arms with electron-donating or -withdrawing groups did not show systematic variance.

Building on the success of the above additivity model, a more complex additivity model was developed to provide a more accurate estimate of the SEs. A multivariate approach was

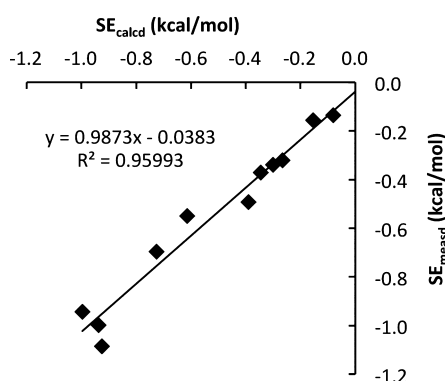


Figure 5. Correlation plot of the calculated (SE_{calcd}) measured (SE_{measd}) SEs for the aromatic stacking interactions in the 11 multisubstituted arms in **1** and **2**. The SE_{calcd} values are based on simple additivity model based on the sum of the individual SE_{measd} values for each multisubstituted arm.

employed similar to that used by Schneider et al. for the analysis of SE additivity in porphyrin host–guest complexes.³⁰ This multivariate model incorporated data from the multisubstituted and monosubstituted arms. Thus, each of the 9 individual SEs (*m*-CH₃, *p*-CH₃, *m*-Cl, *p*-Cl, *m*-CN, *p*-CN, *m*-OCH₃, *p*-OCH₃, *p*-NO₂) were estimated based on multiple SE measurements instead of just the monosubstituted SE measurements used in the previous analysis.

To estimate the 9 individual SEs, a matrix of 21 algebraic equations was created using equation (eq 2) to calculate the SE for each substituted arm in Table 1. Equation 2 calculates the SE for a substituted benzene via the sum of the number of the individual substituents of type *z* (n_z) multiplied by the SE of substituent *z* (SE_z). Using the solver function in Excel, a set of SE_z values was found for the 9 different types of substituents that best fit the SE_{calcd2} and SE_{measd} values for all 21 arms.

$$SE_{\text{calcd2}} = \sum n_z \cdot SE_z \quad (2)$$

The improved accuracy was evident from the better correlation of the SE_{calcd2} and SE_{measd} values. The standard error of the difference was only ± 0.01 kcal/mol. A plot of SE_{measd} versus SE_{calcd2} (Figure 6) also showed the improved correlation with an $R^2 = 0.99$ and a slope was closer to unity

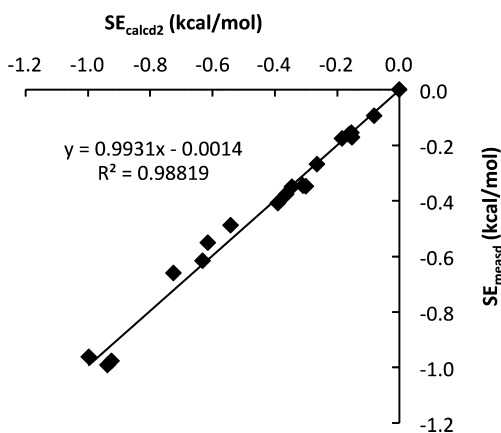


Figure 6. Correlation plot of the measured (SE_{measd}) and calculated SEs (SE_{calcd2}) for all 21 arms using a simple additive model based on the sum of the constituent monosubstituted arms.

(1.00). An additional advantage of this analysis is that it could be used to predict SE_{calcd2} values for monosubstituted arms.

The existence or absence of SE additivity can also be used to test fundamental models of the aromatic stacking interaction. Two general models have been proposed for the origins of the SEs (Figure 7). In the direct interaction model, the substituents

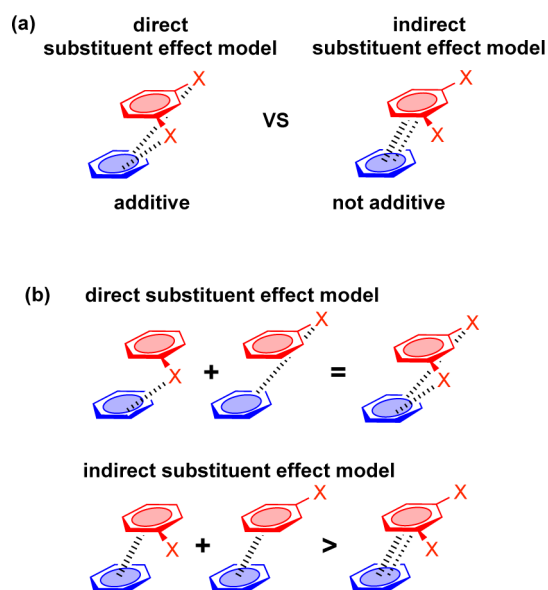


Figure 7. Representations of (a) the direct and indirect SE models for the aromatic stacking interaction and (b) the presence and absence of additive SEs for the direct and indirect SE models.

interact directly with the edges of the opposing aromatic ring.^{27,35,44} Alternatively in the indirect interaction model, the substituents modulate the electrostatic potential of the attached π -system. The polarized aromatic ring, in turn, will have a stronger or weaker electrostatic attraction for the opposing aromatic ring.^{14,45}

The two SE models predict different degrees of SE additivity. The direct model predicts additive SEs.⁴⁴ Each substituent forms a separate interaction with the edge of the opposing aromatic ring. In contrast, the indirect model predicts SEs that are smaller than estimated by an additivity model. In the indirect model, the first substituent will impart the largest electrostatic polarization of the attached π -system. However, each additional substituent has a successively smaller SE as the buildup of charge on the aromatic ring makes the π -surface more difficult to polarize.

Therefore, the additivity of the SEs in our experimental model systems appeared to support the direct SE model. The near unity slopes of the correlation plots (Figures 5 and 6) and trendlines intersecting the origin provide support for the 1:1 correlation of the SE_{measd} to the additivity-based SE_{calcd} values. However, a concern was that the deviation for the indirect model from the additivity model could be too small to be accurately measured. To address this concern, we estimated the deviations from the additivity model for the indirect model by calculating the electrostatic potential (ESP) for a series of benzene rings with varying numbers of substituents (0–6). ESP provides a measure of the electrostatic polarization of the π -system by substituents and was shown by Hunter et al. to correlate to the measured SEs in the aromatic stacking interactions.^{21,24} The ESP calculations were made using the

same method and level of theory (B3LYP, 6-31G*) as used by Hunter et al. Three representative substituents were examined that matched the substituents used in our model system: two electron-withdrawing groups (CN and Cl) and one electron-donating (CH₃) group. ESP for symmetrical substitution patterns is shown in Figure 8 for benzenes bearing 2, 3, and 4 substituents. Similar trends were observed when the ESPs for asymmetric substitution patterns.

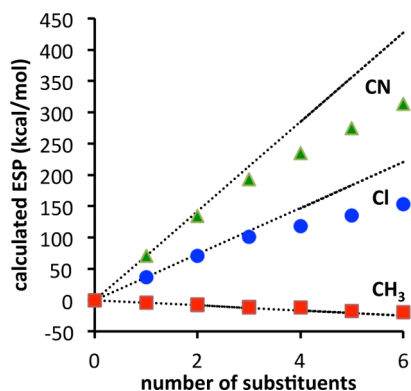


Figure 8. Calculated ESPs (kcal/mol) at the center of benzene rings bearing 0–6 symmetrically positioned substituents (CN, Cl, and CH₃). The broken lines show the expected ESPs for a perfectly additive system.

The ESP calculations showed the expected deviations from additivity (Figure 8). The first substituent had the largest effect, and each successive substituent had a smaller effect. This yielded asymptotic ESP curves that increasingly deviated from the linear additivity model with an increasing number of substituents. However, the deviations from the additivity model were small for benzenes with 2 and 3 substituents, which was the number of substituents in our model systems. The average difference from the additivity model was only -8% with 2 substituents and -11% with 3 substituents. Furthermore, the majority of these differences were due to the electron-donating CH₃ groups that had small SEs, and thus small variations became large percentage differences. Excluding the CH₃ group data, the deviations from the additivity model were only slightly larger than the error in our model system. Therefore, we cannot definitively rule out the indirect SE model.

We examined other ways of differentiating the direct and indirect SE models. Larger deviations ($>20\%$) from the additivity models were predicted for benzenes with 4 or more substituents (Figure 8). However, our current model system is limited to 3 substituents because one position is occupied by the oxygen linker, and the two adjacent *ortho*-positions can form additional steric and dispersion interactions. Alternatively, the distinct SE trends for the *meta*- and *para*-substituents in our model system provide support for the direct SE model. The direct SE model was originally developed for the aligned stacking geometry. However, the direct SE model has also been shown to be applicable to the offset stacking geometry.⁴⁴ A key difference in the offset geometry is that the substituents are no longer symmetrically arranged. Thus, the direct SE model predicts that substituents will have different magnitude SEs depending upon the distance of the substituents from the edge of the opposing aromatic surface. This positional dependence was observed in our system, as the closer *meta*-substituents have a much stronger influence than the *para*-substituents.

Quantitatively, the ratios of the SE for the *meta*- and *para*-positions averaged 1.7:1 as judged by the ratio of the slopes for their Hammett plots (Figure 4).

The indirect model predicts a weaker positional SE dependence than the direct model. To the first approximation, the indirect model should not have a positional dependence, as the *meta*- and *para*-substituents polarize the π -system of the attached aromatic ring to a similar extent. However, the orientation of the polarization of the π -surface will differ depending upon the position of the substituent relative to the dipole or quadrupole of the opposing aromatic surface. Therefore, we cannot entirely rule out the possibility that the indirect model, as the magnitude of its positional dependence is not easily calculated.

CONCLUSIONS

In this study, we have utilized a small molecule model system to experimentally test the additivity of the SEs for the offset stacking aromatic interaction in organic solution. A series of molecular torsional balances **1a–u** and control balances **2a–u** with 21 different substituted benzene arms were prepared containing 5 different substituents (CH₃, OCH₃, Cl, CN, NO₂) that ranged for strongly electron-withdrawing to electron-donating groups. The formation of intramolecular aromatic stacking interactions and the ability to electrostatically influence the interaction energies by the introduction of substituents in our model system were confirmed by NMR, X-ray crystallography, and the observation of linear Hammett plots for the monosubstituted systems. These SEs ranged from slightly destabilizing ($+0.05$ kcal/mol for *p*-CH₃) substituted arm **b** to strongly stabilizing (-1.00 kcal/mol for *m,p*-(CN)₂).

An analysis of the SEs for the 11 multisubstituted balances demonstrated that simple additivity models could provide a good estimate (± 0.01 to ± 0.02 kcal/mol) of the measured SEs. Specifically, the SEs for multisubstituted systems could be accurately estimated from the sum of the individual SEs (eq 2). These individual SEs could be estimated from SE_{measd} of the monosubstituted balances or using via multivariate analysis using the SE_{measd} of the mono- and multisubstituted balances. The observation of SE additivity for the aromatic stacking interaction in this solution-phase study was consistent with previous theoretical studies conducted *in vacuo*.²³

The additivity of SEs for the aromatic stacking interactions has both theoretical and practical applications. First, the SE additivity and the positional dependence of the SEs in our model system provide support for the direct SE model, in which the SEs are due to the direct interaction of the substituents with the edge of the opposing aromatic ring. However, due to the limitation in the number of substituents in our system and the measurement error, we cannot definitively exclude the indirect SE model. Second, the additivity of the SEs for the aromatic stacking interaction has practical applications. This should aid in the rational design and optimization of systems that utilize aromatic stacking, as the magnitude of the stabilization or destabilization by substituents can be accurately predicted using an additive SE model. As demonstrated in this study, the aromatic stacking energies of multisubstituted benzenes can be accurately predicted from the measured stacking energies of the analogous monosubstituted systems. Alternatively, the stacking energies of monosubstituted systems can be predicted from stacking energies of multisubstituted systems. For example from Table 2, the stacking energy of *m*-

CH₃ can be estimated from half of the measured stacking energy of *m,m*-(CH₃)₂.

EXPERIMENTAL SECTION

Measurement of the Folded/Unfolded Ratios. The folding ratios for balances **1a–u** and control balances **2a–u** were measured from the relative peak areas of the succinimide methine protons in the ¹H NMR spectra (CDCl₃, 25 °C, 30 mM) as previously described.^{31,32} Briefly, the peak areas of the succinimide methine singlets in the 4.2 to 4.7 ppm region for the *folded* and *unfolded* conformers were measured using the line fitting method as implemented in the Mnova NMR software. In cases where these peaks overlapped with other protons, the *folded/unfolded* ratios for the succinimide methine protons were verified by comparison with the *folded/unfolded* ratios measured from the most downfield aromatic protons (8.0–8.7 ppm). The *folded* and *unfolded* peaks were assigned based on comparison of their peak areas to the upfield shifted doublet for the *ortho*-proton of the *N*-aryl ring (4.6–4.7 ppm for balance **1**, 5.7–5.8 ppm for balance **2**), which was assigned to the *unfolded* conformer. This peak was assigned to the *unfolded* conformer because this proton is directly over the aromatic shelf in the *unfolded* conformer. The corresponding folding energies (ΔG at 298 K) were calculated from the equation: $\Delta G = -RT \ln[\text{folded}]/[\text{unfolded}]$.

Error Analyses. The error in measuring the *folded/unfolded* ratio from the peak areas in the ¹H NMR spectra was conservatively estimated at $\pm 1\%$ for balances **1a–u**. This estimate is based on the literature studies that have found that concentrations can be accurately measured by ¹H NMR with an accuracy of $< 1\%$.^{46–48} In particular, the use of line shape analysis software can improve the accuracy to $< 0.3\%$ even for overlapped peaks.⁴⁹ To ensure this level of accuracy, the NMR spectra were collected at a high concentration (30 mM). At this concentration, the minor conformer concentration (*folded* or *unfolded*) remained ≥ 10 mM for the entire series of balances **1a–u**.

Despite the measurement of the *folded/unfolded* ratios under similar conditions, a larger measurement error of $\pm 5\%$ was estimated for control balances **2a–u**. Control balances **2a–u** had folding ratios ranging from 1:8 to 1:15. Thus, at 30 mM, the concentration of the minor isomer could be as low as 2 mM. At this lower concentration, we conservatively estimated the peak area measurement error at $\pm 5\%$ based on literature precedent.⁴⁶

Propagation of these measurement errors in the *folded/unfolded* ratios through the Gibbs free energy equation gave errors of ± 0.008 and ± 0.03 kcal/mol for the measured folding energies for **1** and **2** (ΔG_1 and ΔG_2), respectively. Propagation of these errors in ΔG_1 and ΔG_2 through the SE definition equation (eq 1) yielded an error of ± 0.03 kcal/mol in SE_{meas} values.

ASSOCIATED CONTENT

Supporting Information

Experimental details, synthetic procedures, ¹H and ¹³C NMR spectra, X-ray data. This material is available free of charge via the Internet at <http://pubs.acs.org>.

AUTHOR INFORMATION

Corresponding Author

shimizu@mail.chem.sc.edu

Present Address

[†]Tennessee Tech University, Chemistry, Foster Hall (FOST) 107/Box 5055, Cookeville, TN 38505

Notes

The authors declare no competing financial interest.

ACKNOWLEDGMENTS

This work was supported by the National Science Foundation (CHE 1310139, CHE 1048629, and CHE 0911616).

REFERENCES

- (1) Resconi, L.; Cavallo, L.; Fait, A.; Piemontesi, F. *Chem. Rev.* **2000**, *100*, 1253–1345.
- (2) Roesky, H. W.; Andruh, M. *Coord. Chem. Rev.* **2003**, *236*, 91–119.
- (3) Zhao, D. H.; Moore, J. S. *Chem. Commun.* **2003**, 807–818.
- (4) Meyer, E. A.; Castellano, R. K.; Diederich, F. *Angew. Chem., Int. Ed.* **2003**, *42*, 1210–1250.
- (5) Salonen, L. M.; Ellermann, M.; Diederich, F. *Angew. Chem. Int. Ed.* **2011**, *50*, 4808–4842.
- (6) Draper, D. E. *J. Mol. Biol.* **1999**, *293*, 255–270.
- (7) Whitten, D. G.; Chen, L. H.; Geiger, H. C.; Perlstein, J.; Song, X. *D. J. Phys. Chem. B* **1998**, *102*, 10098–10111.
- (8) Riley, K. E.; Hobza, P. *Acc. Chem. Res.* **2013**, *46*, 927–936.
- (9) Klosterman, J. K.; Yamauchi, Y.; Fujita, M. *Chem. Soc. Rev.* **2009**, *38*, 1714–1725.
- (10) Schneider, H. J. *Angew. Chem., Int. Ed.* **2009**, *48*, 3924–3977.
- (11) Moulton, B.; Zaworotko, M. J. *Chem. Rev.* **2001**, *101*, 1629–1658.
- (12) Wei, Y.; Held, I.; Zipse, H. *Org. Biomol. Chem.* **2006**, *4*, 4223–4230.
- (13) Ruano, J. L. G.; Aleman, J.; Alonso, I.; Parra, A.; Marcos, V.; Aguirre, J. *Chem.—Eur. J.* **2007**, *13*, 6179–6195.
- (14) Hunter, C. A.; Sanders, J. K. M. *J. Am. Chem. Soc.* **1990**, *112*, 5525–5534.
- (15) Watt, M.; Hardebeck, L. K. E.; Kirkpatrick, C. C.; Lewis, M. J. *Am. Chem. Soc.* **2011**, *133*, 3854–3862.
- (16) Wheeler, S. E.; McNeil, A. J.; Muller, P.; Swager, T. M.; Houk, K. N. *J. Am. Chem. Soc.* **2010**, *132*, 3304–3311.
- (17) Lee, E. C.; Kim, D.; Jurecka, P.; Tarakeshwar, P.; Hobza, P.; Kim, K. S. *J. Phys. Chem. A* **2007**, *111*, 3446–3457.
- (18) Sinnokrot, M. O.; Sherrill, C. D. *J. Am. Chem. Soc.* **2004**, *126*, 7690–7697.
- (19) Cozzi, F.; Cinquini, M.; Annunziata, R.; Dwyer, T.; Siegel, J. S. *J. Am. Chem. Soc.* **1992**, *114*, 5729–5733.
- (20) Gung, B. W.; Xue, X. W.; Reich, H. J. *J. Org. Chem.* **2005**, *70*, 3641–3644.
- (21) Cockroft, S. L.; Hunter, C. A.; Lawson, K. R.; Perkins, J.; Urch, C. J. *J. Am. Chem. Soc.* **2005**, *127*, 8594–8595.
- (22) Rashkin, M. J.; Waters, M. L. *J. Am. Chem. Soc.* **2002**, *124*, 1860–1861.
- (23) Ringer, A. L.; Sinnokrot, M. O.; Lively, R. P.; Sherrill, C. D. *Chem.—Eur. J.* **2006**, *12*, 3821–3828.
- (24) Cockroft, S. L.; Perkins, J.; Zonta, C.; Adams, H.; Spey, S. E.; Low, C. M. R.; Vinter, J. G.; Lawson, K. R.; Urch, C. J.; Hunter, C. A. *Org. Biomol. Chem.* **2007**, *5*, 1062–1080.
- (25) Ringer, A. L.; Sherrill, C. D. *J. Am. Chem. Soc.* **2009**, *131*, 4574–4575.
- (26) Cozzi, F.; Annunziata, R.; Benaglia, M.; Baldrige, K. K.; Aguirre, G.; Estrada, J.; Sritana-Anant, Y.; Siegel, J. S. *Phys. Chem. Chem. Phys.* **2008**, *10*, 2686–2694.
- (27) Wheeler, S. E.; Houk, K. N. *J. Am. Chem. Soc.* **2008**, *130*, 10854–10855.
- (28) Seo, J.-I.; Kim, I.; Lee, Y. S. *Chem. Phys. Lett.* **2009**, *474*, 101–106.
- (29) Cozzi, F.; Ponzini, F.; Annunziata, R.; Cinquini, M.; Siegel, J. S. *Angew. Chem., Int. Ed. Engl.* **1995**, *34*, 1019–1020.
- (30) Liu, T. J.; Schneider, H. J. *Angew. Chem. Int. Ed.* **2002**, *41*, 1368–1370.
- (31) Carroll, W. R.; Pellechia, P.; Shimizu, K. D. *Org. Lett.* **2008**, *10*, 3547–3550.
- (32) Li, P.; Zhao, C.; Smith, M. D.; Shimizu, K. D. *J. Org. Chem.* **2013**, *78*, 5303–5313.
- (33) Paliwal, S.; Geib, S.; Wilcox, C. S. *J. Am. Chem. Soc.* **1994**, *116*, 4497–4498.
- (34) Mati, I. K.; Cockroft, S. L. *Chem. Soc. Rev.* **2010**, *39*, 4195–4205.
- (35) Arnstein, S. A.; Sherrill, C. D. *Phys. Chem. Chem. Phys.* **2008**, *10*, 2646–2655.

- (36) Nijamudheen, A.; Jose, D.; Shine, A.; Datta, A. *J. Phys. Chem. Lett.* **2012**, *3*, 1493–1496.
- (37) Mooibroek, T. J.; Gamez, P.; Reedijk, J. *CrystEngComm* **2008**, *10*, 1501–1515.
- (38) Hunter, C. A. *Angew. Chem., Int. Ed.* **2004**, *43*, 5310–5324.
- (39) Muchowska, K. B.; Adam, C.; Mati, I. K.; Cockroft, S. L. *J. Am. Chem. Soc.* **2013**, *135*, 9976–9979.
- (40) Hansch, C.; Leo, A.; Taft, R. W. *Chem. Rev.* **1991**, *91*, 165–195.
- (41) Yoshitake, Y.; Misaka, J.; Setoguchi, K.; Abe, M.; Kawaji, T.; Eto, M.; Harano, K. *J. Chem. Soc., Perkin Trans. 2* **2002**, 1611–1619.
- (42) Soininen, P.; Haarala, J.; Vepsalainen, J.; Niemitz, M.; Laatikainen, R. *Anal. Chim. Acta* **2005**, *542*, 178–185.
- (43) Pauli, G. F.; Goedecke, T.; Jaki, B. U.; Lankin, D. C. *J. Nat. Prod.* **2012**, *75*, 834–851.
- (44) Wheeler, S. E. *J. Am. Chem. Soc.* **2011**, *133*, 10262–10274.
- (45) Hunter, C. A.; Lawson, K. R.; Perkins, J.; Urch, C. J. *J. Chem. Soc. Perk. Trans. 2* **2001**, 651–669.
- (46) Rizzo, V.; Pinciroli, V. *J. Pharm. Biomed. Anal.* **2005**, *38*, 851–857.
- (47) Bauer, M.; Bertario, A.; Boccardi, G.; Fontaine, X.; Rao, R.; Verrier, D. *J. Pharm. Biomed. Anal.* **1998**, *17*, 419–425.
- (48) Barding, G. A. J.; Salditos, R.; Larive, C. K. *Anal. Bioanal. Chem.* **2012**, *404*, 1165–1179.
- (49) Soininen, P.; Haarala, J.; Vepsalainen, J.; Niemitz, M.; Laatikainen, R. *Anal. Chim. Acta* **2005**, *542*, 178–185.